

# Orbital Selective Spin Excitations and their Impact on Superconductivity of $\text{LiFe}_{1-x}\text{Co}_x\text{As}$

Yu Li,<sup>1</sup> Zhiping Yin,<sup>2,3,\*</sup> Xiancheng Wang,<sup>4</sup> David W. Tam,<sup>1</sup> D. L. Abernathy,<sup>5</sup> A. Podlesnyak,<sup>5</sup> Chenglin Zhang,<sup>1</sup> Meng Wang,<sup>6</sup> Lingyi Xing,<sup>4</sup> Changqing Jin,<sup>4,7</sup> Kristjan Haule,<sup>3</sup> Gabriel Kotliar,<sup>3,8</sup>  
Thomas A. Maier,<sup>9</sup> and Pengcheng Dai<sup>1,2,†</sup>

<sup>1</sup>Department of Physics and Astronomy, Rice University, Houston, Texas 77005, USA

<sup>2</sup>Center for Advanced Quantum Studies and Department of Physics, Beijing Normal University, Beijing 100875, China

<sup>3</sup>Department of Physics, Rutgers University, Piscataway, New Jersey 08854, USA

<sup>4</sup>Beijing National Laboratory for Condensed Matter Physics, Institute of Physics, Chinese Academy of Sciences, Beijing 100190, China

<sup>5</sup>Quantum Condensed Matter Division, Oak Ridge National Laboratory, Oak Ridge, Tennessee 37831, USA

<sup>6</sup>Department of Physics, University of California, Berkeley, California 94720, USA

<sup>7</sup>Collaborative Innovation Center of Quantum Matter, Beijing, China

<sup>8</sup>Brookhaven National Laboratory, Upton, New York 11973-5000, USA

<sup>9</sup>Center for Nanophase Materials Sciences and Computer Science and Mathematics Division,  
Oak Ridge National Laboratory, Oak Ridge, Tennessee 37831, USA

(Received 18 January 2016; published 17 June 2016)

We use neutron scattering to study spin excitations in single crystals of  $\text{LiFe}_{0.88}\text{Co}_{0.12}\text{As}$ , which is located near the boundary of the superconducting phase of  $\text{LiFe}_{1-x}\text{Co}_x\text{As}$  and exhibits non-Fermi-liquid behavior indicative of a quantum critical point. By comparing spin excitations of  $\text{LiFe}_{0.88}\text{Co}_{0.12}\text{As}$  with a combined density functional theory and dynamical mean field theory calculation, we conclude that wave-vector correlated low energy spin excitations are mostly from the  $d_{xy}$  orbitals, while high-energy spin excitations arise from the  $d_{yz}$  and  $d_{xz}$  orbitals. Unlike most iron pnictides, the strong orbital selective spin excitations in the  $\text{LiFeAs}$  family cannot be described by an anisotropic Heisenberg Hamiltonian. While the evolution of low-energy spin excitations of  $\text{LiFe}_{1-x}\text{Co}_x\text{As}$  is consistent with the electron-hole Fermi surface nesting conditions for the  $d_{xy}$  orbital, the reduced superconductivity in  $\text{LiFe}_{0.88}\text{Co}_{0.12}\text{As}$  suggests that Fermi surface nesting conditions for the  $d_{yz}$  and  $d_{xz}$  orbitals are also important for superconductivity in iron pnictides.

DOI: 10.1103/PhysRevLett.116.247001

Superconductivity in iron pnictides occurs near the vicinity of an antiferromagnetic (AF) instability [1–5]. One exception is  $\text{LiFeAs}$ , which exhibits superconductivity at  $T_c = 18$  K without an AF ordered parent compound [6–8]. Although magnetism is generally believed to play a central role in the superconductivity of iron pnictides [4,5], the unique nature of  $\text{LiFeAs}$  has raised considerable debate concerning whether magnetism is indeed fundamental to the superconductivity of iron-based superconductors. There are two important issues to be addressed. The first is whether magnetism and superconductivity in  $\text{LiFeAs}$  can arise from quasiparticle excitations between hole and electron nested Fermi surfaces similar to other iron pnictide superconductors [9–11]. The second concerns the impact of orbital degrees of freedom on the superconductivity of  $\text{LiFeAs}$  [12,13].

In most iron pnictides, Fe ions are in a  $d^6$  configuration with the five same-spin electrons in the  $e_g$  and  $t_{2g}$  orbitals, and one remaining opposite-spin electron fluctuating among all the  $d$  orbitals, due to the large Hund's rule coupling, although there is a considerable (but smaller) crystal-field splitting between the  $e_g$  and  $t_{2g}$  orbitals [14–20]. The  $t_{2g}$  electrons near the Fermi level occupy the  $d_{xy}$  and degenerate  $d_{xz}/d_{yz}$  orbitals. In the undoped

state, low-energy spin excitations in  $\text{LiFeAs}$  are transversely incommensurate from the AF ordering wave vector of iron pnictides such as  $\text{BaFe}_2\text{As}_2$  [Fig. 1(a) and Fig. 1(b)] [3], consistent with nested Fermi surfaces from either the large  $d_{xy}$  or small  $d_{yz}/d_{xz}$  hole pocket near the  $\Gamma$  point in reciprocal space to electron pockets near  $M$  points [Figs. 1(c) and 1(e)] [21–23]. When Co is doped into  $\text{LiFeAs}$  to form  $\text{LiFe}_{1-x}\text{Co}_x\text{As}$ , superconductivity is gradually suppressed with increasing Co doping and vanishes near  $x = 0.14$  [24], and the system becomes paramagnetic for higher Co-doping levels [Fig. 1(a)] [25]. From angle-resolved photoemission spectroscopy (ARPES) data [26,27], it was found that Co doping introduces electrons to  $\text{LiFeAs}$ , reduces the size of the  $d_{xy}$  hole Fermi surface, moves the small  $d_{yz}/d_{xz}$  hole pockets below the Fermi surface, and enlarges the electron pockets [Fig. 1(d)]. While the hole-electron Fermi surface nesting condition is improved for the  $d_{xy}$  orbitals near  $x = 0.12$ , Fermi surface nesting is no longer possible for the  $d_{yz}/d_{xz}$  orbitals [Fig. 1(d)]. Since transport, optical spectroscopy, and nuclear magnetic resonance measurements on  $\text{LiFe}_{1-x}\text{Co}_x\text{As}$  find enhanced low-energy spin fluctuations near  $x = 0.12$  with non-Fermi liquid behavior, these

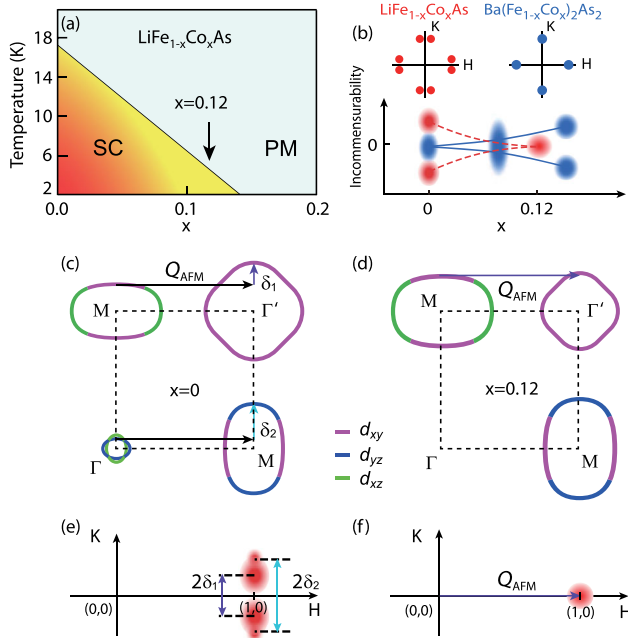


FIG. 1. (a) Electronic phase diagram of  $\text{LiFe}_{1-x}\text{Co}_x\text{As}$ . The superconductivity (SC) is suppressed by Co doping and the system is in paramagnetic (PM) phase above  $T_c$ . The arrow indicates the doping level of  $x = 0.12$  in our experiment [26,27]. (b) Evolution of the low energy spin excitations in reciprocal space with electron doping for LiFeAs and  $\text{BaFe}_2\text{As}_2$ . Red spots indicate positions of low energy spin fluctuations in  $\text{LiFe}_{1-x}\text{Co}_x\text{As}$  and blue ones are for  $\text{BaFe}_{2-x}\text{Ni}_x\text{As}_2$  [28]. Schematics of the Fermi surfaces for LiFeAs (c) and  $\text{LiFe}_{0.88}\text{Co}_{0.12}\text{As}$  (d) [26]. Based on ARPES measurements, the mismatched hole and electron Fermi surfaces should result in the incommensurate spin excitations at  $\delta_1$  and  $\delta_2$ . (e) Positions of transverse incommensurate spin excitations of LiFeAs at  $E = 10$  meV seen in the neutron scattering measurements [23]. (f) Commensurate spin excitations of  $\text{LiFe}_{0.88}\text{Co}_{0.12}\text{As}$  at  $E = 10$  meV.

results were taken as evidence that spin fluctuations due to enhanced Fermi surface nesting can give rise to the observed non-Fermi liquid behavior, but are not important for superconductivity of LiFeAs [25].

In this Letter, we present an inelastic neutron scattering study and a combined density functional theory (DFT) and dynamical mean field theory (DMFT) calculation of spin excitations in  $\text{LiFe}_{0.88}\text{Co}_{0.12}\text{As}$ . While low-energy spin excitations in  $\text{LiFe}_{0.88}\text{Co}_{0.12}\text{As}$  indeed become commensurate consistent with improved electron-hole Fermi surface nesting condition for the  $d_{xy}$  orbitals [Fig. 1(d)], the absence of the hole Fermi pockets near the  $\Gamma$  point prevents the electron-hole nesting between the  $d_{yz}/d_{xz}$  orbitals. Since our DFT + DMFT calculations suggest a strongly correlated  $d_{xy}$  orbital with much reduced magnetic bandwidth and effective exchange coupling (Figs. 2, 3, 4), the improved nesting condition in  $\text{LiFe}_{0.88}\text{Co}_{0.12}\text{As}$ , while sufficient to induce the observed non-Fermi liquid behavior [25] and increased magnetic excitations near the AF wave

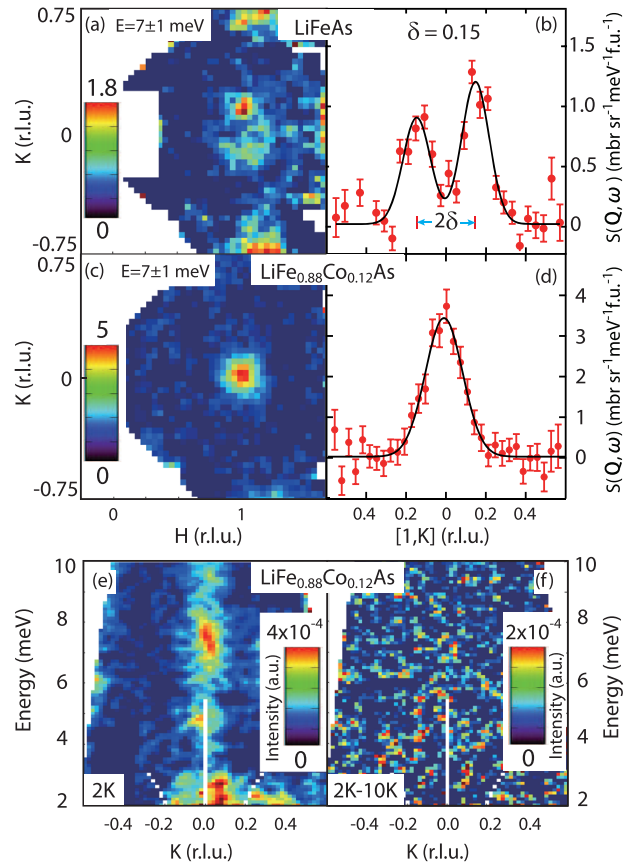


FIG. 2. (a),(c) Two-dimensional constant-energy images of spin excitations in the  $[H, K]$  plane at  $E = 7 \pm 1$  meV and 5 K for LiFeAs and  $\text{LiFe}_{0.88}\text{Co}_{0.12}\text{As}$ , respectively. The high scattering intensity near  $(1, \pm 0.75)$  in (a) is due to phonons, but becomes less obvious in (c) due to different intensity scale. (b),(d) Constant-energy cuts of spin excitations along the  $[1, K]$  direction for LiFeAs and  $\text{LiFe}_{0.88}\text{Co}_{0.12}\text{As}$  at  $E = 7 \pm 1$  meV, respectively. The solid lines are fits to two Gaussians for LiFeAs and a single Gaussian for  $\text{LiFe}_{0.88}\text{Co}_{0.12}\text{As}$  [30]. The intensity is in absolute units by normalizing a vanadium standard. (e) Energy-momentum plots of spin excitations along the  $[1, K]$  direction integrated from  $H = 0.9$  to 1.1 for  $\text{LiFe}_{0.88}\text{Co}_{0.12}\text{As}$ . The commensurate spin excitations form a vertical rod of scattering centered at  $\mathbf{Q}_{AF} = (1, 0)$  point. (f) The temperature difference scattering between 2 and 10 K.

vector, is insufficient to cause superconductivity due to the increased incoherent electronic state of the  $d_{xy}$  band in Co-doped LiFeAs [26]. Similarly, we find that spin excitations at higher energies with much steeper dispersion arise mostly from electron-hole quasiparticle excitations of the  $d_{yz}/d_{xz}$  orbitals with much larger magnetic bandwidth and effective exchange coupling compared with NaFeAs (Fig. 4) [29]. Therefore, spin excitations in the LiFeAs family are highly orbital selective. While spin waves in many iron pnictides can be well described by an anisotropic Heisenberg Hamiltonian [5], the spin excitations in the LiFeAs family cannot be satisfactorily explained by such a model. Our results thus suggest that the occurrence of

superconductivity in  $\text{LiFe}_{1-x}\text{Co}_x\text{As}$  requires Fermi surface nesting of the  $d_{xz}/yz$  orbitals.

Our inelastic neutron scattering measurements on  $\text{LiFeAs}$  and  $\text{LiFe}_{0.88}\text{Co}_{0.12}\text{As}$  were carried out at the wide Angular-Range Chopper Spectrometer (ARCS) and Cold Neutron Chopper Spectrometer (CNCS) at Spallation Neutron Source, Oak Ridge National Laboratory. Single crystals of  $\text{LiFeAs}$  (3.95-g) and  $\text{LiFe}_{0.88}\text{Co}_{0.12}\text{As}$  (7.58-g) are grown using the flux method with the  $^7\text{Li}$  isotope. We define the momentum transfer  $\mathbf{Q}$  in three-dimensional reciprocal space in  $\text{\AA}^{-1}$  as  $\mathbf{Q} = H\mathbf{a}^* + K\mathbf{b}^* + L\mathbf{c}^*$ , where  $H$ ,  $K$ , and  $L$  are Miller indices and  $\mathbf{a}^* = \hat{\mathbf{a}}2\pi/a$ ,  $\mathbf{b}^* = \hat{\mathbf{b}}2\pi/b$ ,  $\mathbf{c}^* = \hat{\mathbf{c}}2\pi/c$  with  $a = b \approx 5.316 \text{ \AA}$ , and  $c = 6.306 \text{ \AA}$  for both samples. In this notation, the AF Bragg peaks for the magnetically ordered compound  $\text{NaFeAs}$  should occur at  $\mathbf{Q}_{\text{AF}} = (\pm 1, 0, L)$  ( $L = 0.5, 1.5, \dots$ ) positions in reciprocal space [Fig. 1(e) and 1(f)] [41]. Samples are coaligned in the  $[H, 0, L]$  scattering plane with mosaic less than  $3^\circ$  and incident beam ( $E_i = 20, 35, 80, 250, 450 \text{ meV}$ ) parallel to the  $c$  axis of the crystals [30].

We first compare low energy spin excitations in pure  $\text{LiFeAs}$  ( $T_c \approx 18 \text{ K}$ ) and  $\text{LiFe}_{0.88}\text{Co}_{0.12}\text{As}$  ( $T_c \approx 4 \text{ K}$ ). Figure 2(a) shows image of the  $E = 7 \pm 1 \text{ meV}$  excitations near  $\mathbf{Q}_{\text{AF}}$  for  $\text{LiFeAs}$  obtained on ARCS. Consistent with earlier work [21–23], the data reveal clear transverse incommensurate spin excitations away from  $\mathbf{Q}_{\text{AF}}$  as shown in the  $[1, K]$  cut of Fig. 2(b). The incommensurate peaks may arise from nesting of the outer hole or inner hole Fermi surface to the electron Fermi surfaces, which give slightly different incommensurability  $\delta_1$  and  $\delta_2$ , respectively, as seen in the experiment [Figs. 1(c) and 1(e)] [22,23]. Figure 2(c) shows an identical image of constant energy ( $E = 7 \pm 1 \text{ meV}$ ) excitations for  $\text{LiFe}_{0.88}\text{Co}_{0.12}\text{As}$ . A constant energy cut along the  $[1, K]$  direction reveals that spin excitations are well defined at the commensurate wave vector  $\mathbf{Q}_{\text{AF}}$  [Fig. 2(d)]. Figure 2(e) shows the dispersion of commensurate spin excitations obtained on CNCS. The rodlike feature at  $\mathbf{Q}_{\text{AF}}$  below 10 meV confirms the commensurate nature of spin excitations in  $\text{LiFe}_{0.88}\text{Co}_{0.12}\text{As}$ . To determine if weak superconductivity at  $T_c = 4 \text{ K}$  has an impact on low-energy spin excitations, we show in Fig. 2(f) temperature difference plot between 2 and 10 K. The absence of the temperature difference scattering in Fig. 2(f) below and above  $T_c$  suggests that the weak superconductivity has negligible effect on the low-energy spin excitations. Based on data in Fig. 2, we summarize in Fig. 1(b) the Co-doping evolution of the low-energy spin excitations in  $\text{LiFe}_{1-x}\text{Co}_x\text{As}$ . Different from  $\text{BaFe}_{2-x}\text{Ni}_x\text{As}_2$ , where the low-energy spin excitations becomes transversely incommensurate with increasing Ni doping [28], Co doping in  $\text{LiFeAs}$  changes transversely incommensurate spin excitations to commensurate as shown in Figs. 1(b), 1(e), and 1(f). The differences in the electron doping evolution of the low-energy spin excitations between  $\text{LiFe}_{1-x}\text{Co}_x\text{As}$  and  $\text{BaFe}_{2-x}\text{Ni}_x\text{As}_2$

can be understood within the Fermi surface nesting picture as due to the differences in Fermi surfaces of  $\text{LiFeAs}$  [26,27] and  $\text{BaFe}_{2-x}\text{As}_2$  [42]. A unique feature of the Fermi surfaces in  $\text{LiFeAs}$  is the large  $d_{xy}$  orbital hole pocket at  $(1,1)$  [Fig. 1(c)] [43]. Upon Co doping to introduce additional electrons to  $\text{LiFeAs}$ , the large  $d_{xy}$  hole pocket shrinks and results in a better nesting with the electron pocket at  $(0,1)$ , while the small  $d_{yz}/d_{xz}$  hole pocket sinks below the Fermi level [Figs. 1(c) and 1(d)]. For  $\text{LiFe}_{0.88}\text{Co}_{0.12}\text{As}$ , the observed commensurate spin excitations are consistent with this picture, and suggest that low-energy spin excitations are mostly driven from the  $d_{xy}$  orbitals. This is consistent with the random phase approximation (RPA) calculations using ARPES determined Fermi surfaces, where the low-energy spin excitations for Co-doped  $\text{LiFeAs}$  involve mostly the  $d_{xy}-d_{xy}$  character (Fig. S3) [30]. Similarly, spin excitations from the  $d_{yz}-d_{yz}$  channel are considerably reduced with the suppression of superconductivity.

Figure 3 summarizes the two-dimensional images of spin excitations at different energies and their comparison with

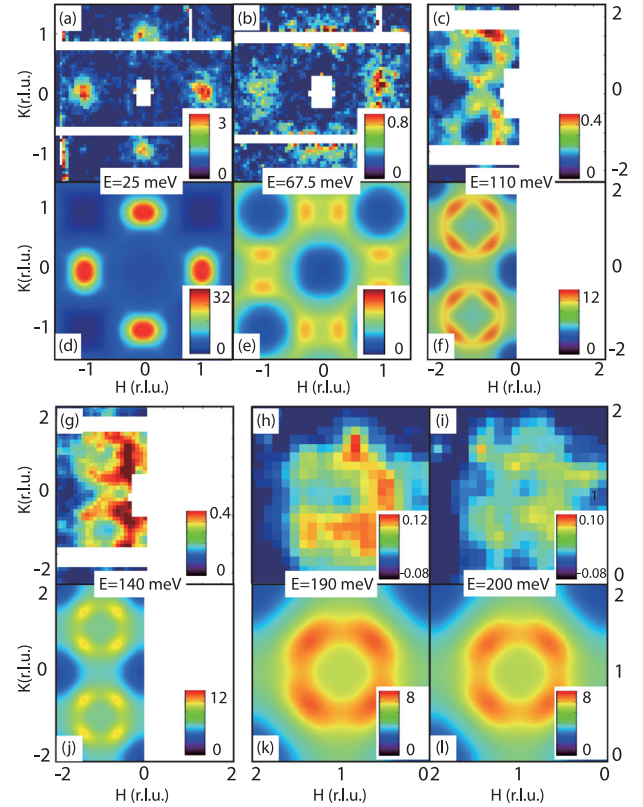


FIG. 3. (a)–(c),(g)–(i) Constant-energy scattering images in the  $[H, K]$  zones for  $\text{LiFe}_{0.88}\text{Co}_{0.12}\text{As}$  at energy transfers of  $E = 25 \pm 5$  ( $E_i = 80$ ),  $67.5 \pm 7.5 \text{ meV}$  ( $E_i = 250 \text{ meV}$ ),  $110 \pm 10$ ,  $140 \pm 10$ ,  $180 \pm 10$ , and  $200 \pm 10 \text{ meV}$  ( $E_i = 450 \text{ meV}$ ). The scattering intensity is obtained after subtracting a radial background and has twofold [(c),(g)] or fourfold symmetry [(h),(i)]. (d)–(f), (j)–(l) Corresponding constant-energy slices of dynamic magnetic structure factor  $S(\mathbf{Q}, E)$  obtained from DFT + DMFT calculation. All data are taken at  $T = 5 \text{ K}$ .

DFT + DMFT calculations for  $\text{LiFe}_{0.88}\text{Co}_{0.12}\text{As}$ . Below  $E = 25$  meV, spin excitations occur at  $\mathbf{Q}_{\text{AF}} = (1, 0)$  and  $(0, 1)$  positions similar to spin waves in  $\text{NaFeAs}$  [Fig. 3(a)] [29]. On increasing energy to  $E = 67.5 \pm 7.5$  meV, spin excitations begin to split vertically from  $(1, 0)$ , again similar to spin waves of  $\text{NaFeAs}$  [Fig. 3(b)]. However, at energies above  $E = 100$  meV, spin excitations in  $\text{LiFe}_{0.88}\text{Co}_{0.12}\text{As}$  form rings of scattering centered around  $(\pm 1, \pm 1)$  which shrink slowly with increasing energy and persist up to  $E = 200$  meV [Figs. 3(c), 3(g), 3(h), and 3(i)]. This is significantly different from  $\text{NaFeAs}$ , where spin waves reach the band top near 100 meV [29]. Since high-energy spin excitations in  $\text{LiFeAs}$  behave similarly [44], we conclude that spin excitations of  $\text{LiFe}_{1-x}\text{Co}_x\text{As}$  have larger bandwidth than that of  $\text{NaFeAs}$  [29], are similar to that of  $\text{BaFe}_{2-x}\text{Ni}_x\text{As}_2$  [45,46]. Given the similar crystal structure and superconducting transition temperatures of  $\text{LiFe}_{1-x}\text{Co}_x\text{As}$  [24] and  $\text{NaFe}_{1-x}\text{Co}_x\text{As}$  [47], one would expect similar electron correlation and spin excitation bandwidth in these two families of materials [48,49].

To determine the spin excitation dispersions of  $\text{LiFe}_{0.88}\text{Co}_{0.12}\text{As}$ , we made a series of cuts on images of spin excitations in Fig. 3 along the  $[1, K]$  direction at different energies (Fig. S2) [30] and extracted the dispersion as shown in Fig. 4(a). Compared with dispersions of spin waves in  $\text{NaFeAs}$  [29] and spin excitations in  $\text{BaFe}_{2-x}\text{Ni}_x\text{As}_2$  [45,46], dispersion of  $\text{LiFe}_{0.88}\text{Co}_{0.12}\text{As}$  has distinctive features around 100 meV [Fig. 4(a)]. Figure 4(b) shows the DFT + DMFT calculated total dynamic spin dynamic susceptibility, which reveals clear two component structures similar to spin excitations in Fig. 4(a). Figures 4(c), 4(d), and 4(e) show dynamic spin susceptibility corresponding to the  $d_{xy}$ - $d_{xy}$ ,  $d_{xz}$ - $d_{xz}$ , and  $d_{yz}$ - $d_{yz}$  intraorbital scattering channels between the hole and electron Fermi surfaces, respectively. Along the  $(1, K)$  direction, spin excitations from the  $d_{xy}$  orbital reach zone boundary around  $E = 130$  meV [Fig. 4(c)], while excitations from the  $d_{yz}$  orbital extend to energies well above  $E = 200$  meV [along the  $(K, 1)$  direction, it would be the  $d_{xz}$  orbital component due to the fourfold symmetry]. The similarities in Figs. 4(a) and 4(b) strongly suggest that the upper and lower branches of the observed spin excitations have different orbital origins. In Fig. 4(f), we compare the estimated local dynamic spin susceptibility for  $\text{LiFe}_{0.88}\text{Co}_{0.12}\text{As}$  and  $\text{LiFeAs}$  at  $T = 5$  K. The total fluctuating moment of  $\text{LiFe}_{0.88}\text{Co}_{0.12}\text{As}$  is  $\langle \mathbf{m}^2 \rangle = 1.5 \pm 0.3 \mu_B^2/\text{Fe}$ . This is similar to superconducting  $\text{LiFeAs}$  [21–23], but is somewhat smaller than those of  $\text{NaFeAs}$  ( $\langle \mathbf{m}^2 \rangle \approx 3.2 \mu_B^2/\text{Fe}$ ) [29] and  $\text{BaFe}_2\text{As}_2$  ( $\langle \mathbf{m}^2 \rangle \approx 3.6 \mu_B^2/\text{Fe}$ ) [50,51]. This means that the total fluctuating moments for the  $\text{LiFeAs}$  family of materials are smaller than those of  $\text{NaFeAs}$  and  $\text{BaFe}_2\text{As}_2$  iron pnictides.

In iron pnictide such as  $\text{BaFe}_2\text{As}_2$ , spin wave dispersions can be well described by an anisotropic Heisenberg Hamiltonian [50]. However, the two branch feature of the spin excitation dispersion in  $\text{LiFe}_{0.88}\text{Co}_{0.12}\text{As}$  clearly

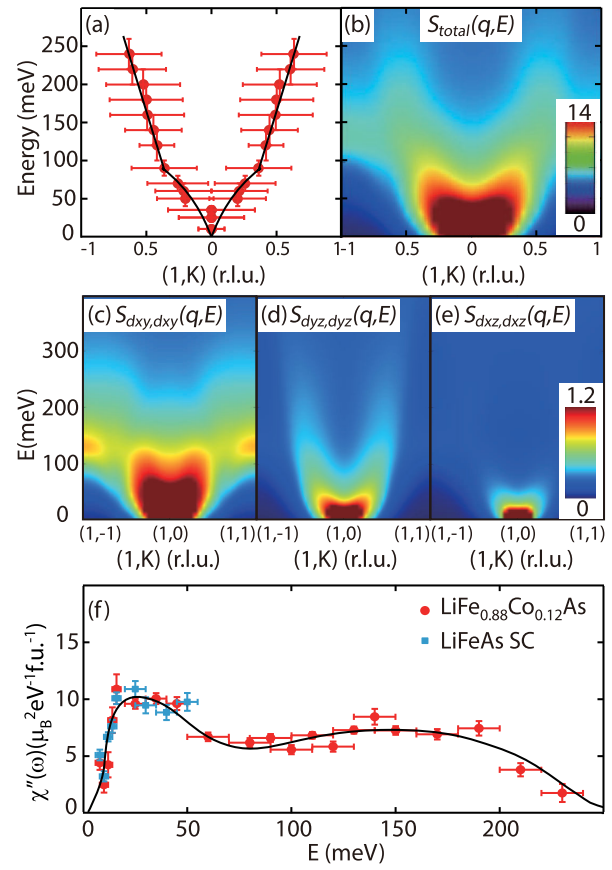


FIG. 4. (a) The dispersion of spin excitations from time-of-flight neutron scattering data as seen in Fig. S2 [30]. The points represent the peak positions fitted with Gaussians. The errors in energy are the energy integration range and the  $\mathbf{Q}$ -errors come from the fitted peak width. (b) The corresponding total dynamic spin susceptibility calculated by DFT + DMFT. (c)–(e) The diagonal components of the dynamic magnetic structure factor  $S_{xy,xy}(\mathbf{q}, E)$ ,  $S_{yz,yz}(\mathbf{q}, E)$ , and  $S_{xz,xz}(\mathbf{q}, E)$  which originate from the  $d_{xy}$ ,  $d_{yz}$  and  $d_{xz}$  orbitals, respectively. (f) Energy dependence of the measured local dynamic spin susceptibility for  $\text{LiFe}_{0.88}\text{Co}_{0.12}\text{As}$  and superconducting  $\text{LiFeAs}$  at  $T = 5$  K.

cannot be satisfactorily fitted by this anisotropic Heisenberg model. Our neutron scattering experiments and DFT + DMFT calculations suggest that orbital selective quasiparticle excitations may account for the energy and wave vector dependence of spin excitations in  $\text{LiFe}_{0.88}\text{Co}_{0.12}\text{As}$ . This indicates that the superexchange spin interactions are different for different orbitals.

It is well known that electronic correlations in iron pnictides depend sensitively on the Fe pnictogen distance owing to the kinetic frustration mechanism of the Fe 3d electrons, and are strongly enhanced with increasing Fe-pnictogen distance [48,49,52]. Together with the large Hund's rule coupling and strong on-site Coulomb repulsion, the kinetic frustration mechanism also gives rise to the strong orbital differentiation of the electronic correlation strength [15,48]. Orbital selective electronic correlation has

been found in  $\text{FeTe}_{1-x}\text{Se}_x$ , where the effective mass of bands dominated by the  $d_{xy}$  orbital character decreases with increasing selenium as compared to the  $d_{xz}/d_{yz}$  bands [53]. In the case of LiFeAs, charge transfer from the  $d_{xy}$  to  $d_{xz}/d_{yz}$  orbitals can account for the Fermi surface topology of LiFeAs as the consequence of orbital dependent band renormalization [48,54]. As shown in Fig. S6 [30], the increased pnictogen height in LiFeAs compared with NaFeAs narrows the electronic bandwidth of the  $d_{xy}$  orbital, which in turn transfers electrons from the  $d_{xy}$  to the  $d_{xz}/d_{yz}$  bands. The observed Co-doping dependence of low-energy spin excitations results from the  $d_{xy}$ - $d_{xy}$  orbital dependent Fermi surface nesting. The narrow electronic bandwidth of the  $d_{xy}$  also leads to narrow bandwidth of spin excitations, and weak effective magnetic exchange coupling.

Since the  $d_{xy}$  orbital dominated Fermi surface nesting becomes better for  $\text{LiFe}_{0.88}\text{Co}_{0.12}\text{As}$ , low-energy spin excitations become commensurate with enhanced spectral weight compared to incommensurate spin excitations in LiFeAs [Figs. 1(b) and 1(d)]. This is consistent with NMR measurements [25] and RPA/DFT + DMFT calculations (Figs. S3 and S4) [30]. The observed non-Fermi liquid behavior near  $x = 0.12$  is then due to vanishing Fermi surface pocket associated with  $d_{yz}/d_{xz}$  orbitals as the Lifshitz transition is approached from the underdoped side [55]. In principle, an increased spin-fluctuation spectral weight should provide a larger electron pairing strength, and thus higher  $T_c$  within the spin-fluctuation mediated superconductivity scenario [4]. However, since Co doping to LiFeAs also induces large incoherent electron scattering [26] and narrows the magnetic bandwidth in the  $d_{xy}$  orbital [Fig. 4(c)], superconductivity associated with the  $d_{xy}$  orbital may be prohibited due to reduced effective magnetic exchange coupling associated with the  $d_{xy}$  orbitals [56]. Similarly, in spite of the large magnetic bandwidth associated with the  $d_{xz}/d_{yz}$  orbitals, the poor Fermi surface nesting of these orbitals suppresses low energy spin excitations, which is also bad for superconductivity [56]. Therefore, superconductivity in iron pnictides can only occur with appropriate orbital selective low-energy spin excitations coupled with reasonable large magnetic exchange coupling.

The neutron scattering work at Rice is supported by the U.S. DOE, BES DE-SC0012311 (P. D.). The computational work at Rice, ORNL, and Rutgers is supported by NSF DMR-1436006 (P. D.), DMR-1308603 (T. M.), DMR-1405303 (K. H.), and DMR-1435918 (Z. P. Y. and G. K.). The materials effort at Rice is also supported by the Robert A. Welch Foundation Grant No. C-1839 (P. D.). The research at SNS was sponsored by the Scientific User Facilities Division, BES, U.S. DOE. The research used resources of the Oak Ridge Leadership Computing Facility at ORNL, which is supported by U.S. DOE under Contract No. DE-AC05-00OR22725. The work at IOP, CAS is supported by NSFC and MOST of China through research projects.

\*yinzhiping@bnu.edu.cn

<sup>†</sup>pdai@rice.edu

- [1] Y. Kamihara, T. Watanabe, M. Hirano, and H. Hosono, *J. Am. Chem. Soc.* **130**, 3296 (2008).
- [2] C. de la Cruz, Q. Huang, J. W. Lynn, J. Li, W. Ratcliff II, J. L. Zarestky, H. A. Mook, G. F. Chen, J. L. Luo, N. L. Wang, and P. C. Dai, *Nature (London)* **453**, 899 (2008).
- [3] Q. Huang, Y. Qiu, Wei Bao, M. A. Green, J. W. Lynn, Y. C. Gasparovic, T. Wu, G. Wu, and X. H. Chen, *Phys. Rev. Lett.* **101**, 257003 (2008).
- [4] D. J. Scalapino, *Rev. Mod. Phys.* **84**, 1383 (2012).
- [5] P. C. Dai, *Rev. Mod. Phys.* **87**, 855 (2015).
- [6] X. Wang, Q. Liu, Y. Lv, W. Gao, L. Yang, R. Yu, F. Li, and C. Jin, *Solid State Commun.* **148**, 538 (2008).
- [7] M. J. Pitcher, D. R. Parker, P. Adamson, S. J. C. Herkelrath, A. T. Boothroyd, R. M. Ibberson, M. Brunelli, and S. J. Clarke, *Chem. Commun. (Cambridge)* **45**, 5918 (2008).
- [8] J. H. Tapp, Z. J. Tang, B. Lv, K. Sasmal, B. Lorenz, P. C. W. Chu, and A. M. Guloy, *Phys. Rev. B* **78**, 060505(R) (2008).
- [9] P. J. Hirschfeld, M. M. Korshunov, and I. I. Mazin, *Rep. Prog. Phys.* **74**, 124508 (2011).
- [10] A. V. Chubukov, *Annu. Rev. Condens. Matter Phys.* **3**, 57 (2012).
- [11] Y. Wang, A. Kreisel, V. B. Zabolotnyy, S. V. Borisenko, B. Büchner, T. A. Maier, P. J. Hirschfeld, and D. J. Scalapino, *Phys. Rev. B* **88**, 174516 (2013).
- [12] T. Saito, S. Onari, Y. Yamakawa, H. Kontani, S. V. Borisenko, and V. B. Zabolotnyy, *Phys. Rev. B* **90**, 035104 (2014).
- [13] T. Saito, Y. Yamakawa, S. Onari, and H. Kontani, *Phys. Rev. B* **92**, 134522 (2015).
- [14] K. Haule and G. Kotliar, *New J. Phys.* **11**, 025021 (2009).
- [15] A. Georges, L. De Medici, and J. Mravlje, *Annu. Rev. Condens. Matter Phys.* **4**, 137 (2013).
- [16] C. C. Lee, W. G. Yin, and W. Ku, *Phys. Rev. Lett.* **103**, 267001 (2009).
- [17] F. Krüger, S. Kumar, J. Zaanen, and J. van den Brink, *Phys. Rev. B* **79**, 054504 (2009).
- [18] W. C. Lv, J. S. Wu, and P. Phillips, *Phys. Rev. B* **80**, 224506 (2009).
- [19] C.-C. Chen, J. Maciejko, A. P. Sorini, B. Moritz, R. R. P. Singh, and T. P. Devereaux, *Phys. Rev. B* **82**, 100504(R) (2010).
- [20] B. Valenzuela, E. Bascones, and M. J. Calderón, *Phys. Rev. Lett.* **105**, 207202 (2010).
- [21] N. Qureshi, P. Steffens, Y. Drees, A. C. Komarek, D. Lamago, Y. Sidis, L. Harnagea, H.-J. Grafe, S. Wurmehl, B. Büchner, and M. Braden, *Phys. Rev. Lett.* **108**, 117001 (2012).
- [22] M. Wang, M. Y. Wang, H. Miao, S. V. Carr, D. L. Abernathy, M. B. Stone, X. C. Wang, L. Y. Xing, C. Q. Jin, X. T. Zhang, J. P. Hu, T. Xiang, H. Ding, and P. C. Dai, *Phys. Rev. B* **86**, 144511 (2012).
- [23] N. Qureshi, P. Steffens, D. Lamago, Y. Sidis, O. Sobolev, R. A. Ewings, L. Harnagea, S. Wurmehl, B. Büchner, and M. Braden, *Phys. Rev. B* **90**, 144503 (2014).
- [24] M. J. Pitcher, T. Lancaster, J. D. Wright, I. Franke, A. J. Steele, P. J. Baker, F. L. Pratt, W. T. Thomas, D. R. Parker, S. J. Blundell *et al.*, *J. Am. Chem. Soc.* **132**, 10467 (2010).

- [25] Y. M. Dai, H. Miao, L. Y. Xing, X. C. Wang, P. S. Wang, H. Xiao, T. Qian, P. Richard, X. G. Qiu, W. Yu, C. Q. Jin, Z. Wang, P. D. Johnson, C. C. Homes, and H. Ding, *Phys. Rev. X* **5**, 031035 (2015).
- [26] Z. R. Ye, Y. Zhang, F. Chen, M. Xu, J. Jiang, X. H. Niu, C. H. P. Wen, L. Y. Xing, X. C. Wang, C. Q. Jin, B. P. Xie, and D. L. Feng, *Phys. Rev. X* **4**, 031041 (2014).
- [27] H. Miao, T. Qian, X. Shi, P. Richard, T. K. Kim, M. Hoesch, L. Y. Xing, X.-C. Wang, C.-Q. Jin, J.-P. Hu, and H. Ding, *Nat. Commun.* **6**, 6056 (2015).
- [28] H. Q. Luo, Z. Yamani, Y. Chen, X. Y. Lu, M. Wang, S. L. Li, T. A. Maier, S. Danilkin, D. T. Adroja, and P. C. Dai, *Phys. Rev. B* **86**, 024508 (2012).
- [29] C. L. Zhang, L. W. Harriger, Z. P. Yin, W. C. Lv, M. Y. Wang, G. T. Tan, Y. Song, D. L. Abernathy, W. Tian, T. Egami, K. Haule, G. Kotliar, and P. C. Dai, *Phys. Rev. Lett.* **112**, 217202 (2014).
- [30] See Supplemental Material at <http://link.aps.org/supplemental/10.1103/PhysRevLett.116.247001> for information on sample preparation, neutron data analysis, RPA and DMFT calculations, which includes Refs. [31–40].
- [31] L. Y. Xing, H. Miao, X. C. Wang, J. Ma, Q. Q. Liu, Z. Deng, H. Ding, and C. Q. Jin, *J. Phys. Condens. Matter* **26**, 435703 (2014).
- [32] D. R. Parker, M. J. Pitcher, P. J. Baker, I. Franke, T. Lancaster, S. J. Blundell, and S. J. Clarke, *Chem. Commun. (Cambridge)* **16**, 2189 (2009).
- [33] H. Eschrig and K. Koepernik, *Phys. Rev. B* **80**, 104503 (2009).
- [34] K. Kuroki, S. Onari, R. Arita, H. Usui, Y. Tanaka, H. Kontani, and H. Aoki, *Phys. Rev. Lett.* **101**, 087004 (2008).
- [35] P. Blaha, K. Schwarz, G. K. H. Madsen, D. Kvasnicka, and J. Luitz, WIEN2K (K. Schwarz, Techn. Univ. Wien, Austria, 2001).
- [36] J. P. Perdew, K. Burke, and M. Ernzerhof, *Phys. Rev. Lett.* **77**, 3865 (1996).
- [37] G. Kotliar, S. Y. Savrasov, K. Haule, V. S. Oudovenko, O. Parcollet, and C. A. Marianetti, *Rev. Mod. Phys.* **78**, 865 (2006).
- [38] K. Haule, C.-H. Yee, and K. Kim, *Phys. Rev. B* **81**, 195107 (2010).
- [39] K. Haule, *Phys. Rev. B* **75**, 155113 (2007).
- [40] P. Werner, A. Comanac, L. de Medici, M. Troyer, and A. J. Millis, *Phys. Rev. Lett.* **97**, 076405 (2006).
- [41] S. L. Li, C. de la Cruz, Q. Huang, G. F. Chen, T.-L. Xia, J. L. Luo, N. L. Wang, and P. C. Dai, *Phys. Rev. B* **80**, 020504(R) (2009).
- [42] M. Yi, D. H. Lu, J.-H. Chu, J. G. Analytis, A. P. Sorini, A. F. Kemper, B. Moritz, S.-K. Mo, R. G. Moore, M. Hashimoto, W.-S. Lee, Z. Hussain, T. P. Devereaux, I. R. Fisher, and Z.-X. Shen, *Proc. Natl. Acad. Sci. U.S.A.* **108**, 6878 (2011).
- [43] S. V. Borisenko, V. B. Zabolotnyy, D. V. Evtushinsky, T. K. Kim, I. V. Morozov, A. N. Yaresko, A. A. Kordyuk, G. Behr, A. Vasiliev, R. Follath, and B. Buchner, *Phys. Rev. Lett.* **105**, 067002 (2010).
- [44] Meng Wang, X. C. Wang, D. L. Abernathy, L. W. Harriger, H. Q. Luo, Yang Zhao, J. W. Lynn, Q. Q. Liu, C. Q. Jin, C. Fang, J. P. Hu, and P. C. Dai, *Phys. Rev. B* **83**, 220515(R) (2011).
- [45] M. S. Liu, L. W. Harriger, H. Q. Luo, M. Wang, R. A. Ewings, T. Guidi, H. Park, K. Haule, G. Kotliar, S. M. Hayden, and P. C. Dai, *Nat. Phys.* **8**, 376 (2012).
- [46] H. Q. Luo, X. Y. Lu, R. Zhang, M. Wang, E. A. Goremychkin, D. T. Adroja, S. Danilkin, G. Deng, Z. Yamani, and P. C. Dai, *Phys. Rev. B* **88**, 144516 (2013).
- [47] D. R. Parker, M. J. P. Smith, T. Lancaster, A. J. Steele, I. Franke, P. J. Baker, F. L. Pratt, M. J. Pitcher, S. J. Blundell, and S. J. Clarke, *Phys. Rev. Lett.* **104**, 057007 (2010).
- [48] Z. P. Yin, K. Haule, and G. Kotliar, *Nat. Mater.* **10**, 932 (2011).
- [49] Z. P. Yin, K. Haule, and G. Kotliar, *Nat. Phys.* **10**, 845 (2014).
- [50] L. W. Harriger, H. Q. Luo, M. S. Liu, C. Frost, J. P. Hu, M. R. Norman, and P. C. Dai, *Phys. Rev. B* **84**, 054544 (2011).
- [51] L. W. Harriger, M. Liu, H. Luo, R. A. Ewings, C. D. Frost, T. G. Perring, and P. C. Dai, *Phys. Rev. B* **86**, 140403(R) (2012).
- [52] Y. K. Kim, Y. Y. Koh, W. S. Kyung, G. R. Han, B. Lee, Kee Hoon Kim, J. M. Ok, Jun Sung Kim, M. Arita, K. Shimada, H. Namatame, M. Taniguchi, S.-K. Mo, and C. Kim, *Phys. Rev. B* **92**, 041116(R) (2015).
- [53] Z. K. Liu, M. Yi, Y. Zhang, J. Hu, R. Yu, J.-X. Zhu, R.-H. He, Y. L. Chen, M. Hashimoto, R. G. Moore, S.-K. Mo, Z. Hussain, Q. Si, Z. Q. Mao, D. H. Lu, and Z.-X. Shen, *Phys. Rev. B* **92**, 235138 (2015).
- [54] Geunsik Lee, Hyo Seok Ji, Yeongkwan Kim, Changyoung Kim, Kristjan Haule, Gabriel Kotliar, Bumsung Lee, Seunghyun Khim, Kee Hoon Kim, Kwang S. Kim, Ki-Seok Kim, and Ji Hoon Shim, *Phys. Rev. Lett.* **109**, 177001 (2012).
- [55] S. D. Das, M. S. Laad, L. Craco, J. Gillett, V. Tripathi, and S. E. Sebastian, *Phys. Rev. B* **92**, 155112 (2015).
- [56] M. Wang, C. L. Zhang, X. Y. Lu, G. T. Tan, H. Q. Luo, Y. Song, M. Y. Wang, X. T. Zhang, E. A. Goremychkin, T. G. Perring, T. A. Maier, Z. P. Yin, K. Haule, G. Kotliar, and P. C. Dai, *Nat. Commun.* **4**, 2874 (2013).